Article

Not peer-reviewed version

Synthesis, Structural and Luminescent Properties of TmMgB5O10 Crystals

Elena A. Volkova *, Victor V. Maltsev, Alexander M. Antipin, Dina V. Deineko, Ivan V. Nikiforov, Ekaterina I. Marchenko, Diana D. Mitina, Vladimir L. Kosorukov, Vasiliy O. Yapaskurt, Daniil A. Naprasnikov, Elizaveta . V Koporulina

Posted Date: 30 August 2023

doi: 10.20944/preprints202308.2036.v1

Keywords: borates; flux growth; crystal structure; electronic band; differential scanning calorimetry; photoluminescence

Article

Synthesis, Structural and Luminescent Properties of $TmMgB_5O_{10}$ Crystals

Elena A. Volkova [1,*], Victor V. Maltsev [1], Alexander M. Antipin [2], Dina V. Deineko [3], Ivan V. Nikiforov [3], Dmitry A. Spassky [4,5], Ekaterina I. Marchenko [1], Diana D. Mitina [1], Vladimir L. Kosorukov [1], Vasiliy O. Yapaskurt [1], Daniil A. Naprasnikov [1] and Elizaveta V. Koporulina [1,6]

[1] Faculty of Geology, Moscow State University, 119991 Moscow, Russia; volkova@geol.msu.ru (E.A.V.); maltsev@geol.msu.ru (V.V.M.); marchenko-ekaterina@bk.ru (E.I.M), varya-mitya@mail.ru (D.D.M.), daniilnaprasnikov@mail.ru (D.A.N.), kosorukov-vladimir@rambler.ru (V.L.K.), vyapaskurt@mail.ru (V.O.Y.), e_koporulina@mail.ru (E.V.K)

[2] Shubnikov Institute of Crystallography of Federal Scientific Research Centre «Crystallography and Photonics» of Russian Academy of Sciences, 119333 Moscow, Russia; antipin@physics.msu.ru (A.M.A.)

[3] Faculty of Chemistry, Moscow State University, 119991 Moscow, Russia; deynekomsu@gmail.com (D.V.D.) nikiforoviv@my.msu.com (I.V.N.)

[4] Skobeltsyn Institute of Nuclear Physics, Lomonosov Moscow State University, 119991 Moscow, Russia; spas@srd.sinp.msu.ru (D.A.S)

[5] Institute of Physics, University of Tartu, 50411 Tartu, Estonia

[6] Melnikov Research Institute of Comprehensive Exploitation of Mineral Resources of the Russian Academy of Sciences, 111020 Moscow, Russia

* Correspondence: volkova@geol.msu.ru

Abstract: $TmMgB_5O_{10}$ spontaneous crystals were synthesized *via* flux-growth technique from a $K_2Mo_3O_{10}$-based solvent. The crystal structure of the compound was solved and refined within the space group $P2_1/n$. The first principles calculations of the electronic structure reveal that TmMg-pentaborate with an ideal not defected crystal structure is an insulator with an indirect energy band gap of approximately 6.37 eV. Differential scanning calorimetry measurements and powder X-ray diffraction studies of heat-treated solids show that $TmMgB_5O_{10}$ is an incongruent melting compound. A characteristic band of Tm^{3+} cation corresponding to the $^3H_6 \rightarrow {}^1D_2$ transition is observed in the photoluminescence excitation spectra of TmMg-borate. The as-obtained crystals exhibit intense blue emission with the emission peaks centered at 455, 479, 667 and 753 nm. The most intensive band corresponds to the $^1D_2 \rightarrow {}^3F_4$ transition. $TmMgB_5O_{10}$ solids demonstrate thermal stability of photoluminescence.

Keywords: borates; flux growth; crystal structure; electronic band; differential scanning calorimetry; photoluminescence

1. Introduction

In recent decades, a large amount of research is focused on the development of materials used as environmentally friendly light sources and phosphors, as well as laser and nonlinear optical materials. Future progress in science and technology is directly related to the search and further application of new compounds, as well as to the improvement of the parameters of existing materials. One of the promising classes of such compounds is rare-earth borates, which demonstrate high chemical stability, thermal and radiation resistance, wide transparency area, high laser threshold and *etc*. In addition, borates have a wide variety of chemical compositions and crystal structures due to the ability of the boron atom to form various anionic and polyanionic groups [1]. Nowadays, the search of borates materials that can be used as phosphors is an actual problem. There are many borate crystals that do not exhibit luminescent properties in their pure form, and their luminescent characteristics are associated with doping, such as incorporation of rare-earth or transition metal cations into their structure.

Preprints (www.preprints.org) | NOT PEER-REVIEWED | Posted: 30 August 2023 doi:10.20944/preprints202308.2036.v1

In particular, among numerous borates, a group of rare-earth magnesium pentaborates can be used as phosphors to create powerful emitters of the visible range with ultraviolet (UV) excitation [2,3]. Rare-earth magnesium borates with the general chemical formula $LnMgB_5O_{10}$ (where *Ln* = La, Ce-Nd, Sm-Er) were first synthesized by Saubat *et al.* in 1980 by solid-phase method. $LaMgB_5O_{10}$ single crystals were then obtained by melting a mixture of La_2O_3, MgO and B_2O_3 at 1200 °C with an excess of magnesium and boron oxides with respect to the stoichiometric amount to compensate for volatilization losses. The crystal structure of $LaMgB_5O_{10}$ was solved and refined within the space group (sp.gr.) $P2_1/c$ [4]. The powder patterns of other polycrystalline $LnMgB_5O_{10}$ samples were also indexed in the same space group. These materials exhibit remarkable structural features: a weak atomic *Ln*/O ratio, well isolated *Ln* chains, separated by large polyborate anions along with a highly covalent matrix suggest the possibility of relatively low-concentration quenching. $LnMgB_5O_{10}$ is expected to be an excellent material as phosphor hosts and a matrix for solid-state laser.

The luminescent properties of this group of compounds were first described by the authors of [5,6] for $LaMgB_5O_{10}$ alloyed with Eu^{3+}, Tb^{3+}, and Ce^{3+}. Luminescence parameters of Ce^{3+}:$LaMgB_5O_{10}$ and Ce^{3+}:$YMgB_5O_{10}$ powders [7], nanocrystalline $(La,Gd)MgB_5O_{10}$:Ce^{3+}/Tb^{3+} thin films synthesized by sol-gel method [8], and $LaMgB_5O_{10}$ – based glasses, doped with Ce^{3+}, Tb^{3+}, and Mn^{2+} were studied later [9]. Recently, data on the luminescence of LaMg-pentaborate crystals doped with Tb^{3+} and Eu^{3+} ions were obtained by the authors of Ref. [3]. There are also a number of investigations on the characterization of large-size and high-quality $LaMgB_5O_{10}$, $GdMgB_5O_{10}$, and $YMgB_5O_{10}$ laser crystals doped with Yb^{3+}, Er^{3+}, Nd^{3+} (see, for example, Ref. [5–9]). Based on the analysis of spectra and laser characteristics, it was shown that these borates are promising candidates for multi-wavelength laser crystals.

A review of previous studies on the synthesis and crystal growth of rare-earth pentaborates shows that the Li_2O–B_2O_3–LiF mixed flux is the most commonly used to obtain $LnMgB_5O_{10}$ compounds by the solution growth on dipped seeds technique [10,11]. Recently, $GdMgB_5O_{10}$

single crystals were obtained from $K_2Mo_3O_{10}$ flux [12]. The authors of Refs. [13,14] performed experiments in Li_2O–B_2O_3–LiF and $K_2Mo_3O_{10}$ –based systems to determine the most suitable one for growth of $LnMgB_5O_{10}$ bulk crystals. It was shown that $K_2Mo_3O_{10}$ flux is preferable. The strong tendency of Li_2O-B_2O_3-LiF melts to glass formation, and high volatility and reactivity of fluorides at high temperatures make reproducible growth of high-quality crystals difficult. It was also proposed to use pre-synthesized $LnMgB_5O_{10}$ tablets as a crystal-forming agent instead of the mixture of corresponding Ln_2O_3–MgO–B_2O_3 oxides.

Spontaneous $TmMgB_5O_{10}$ (TmMB) single crystals were obtained for the first time in the framework of the approach described in [14]. The present work is focused on synthesis and study of the crystal structure, thermal behavior, and luminescent properties of $TmMgB_5O_{10}$ crystals.

2. Materials and Methods

Two subsequent routes were applied to obtain TmMg-borate: solid-state synthesis and flux-growth techniques. In both cases, a vertical resistance-heated furnace equipped with a Proterm-100 precision temperature controller and a set of Pt/Rh-Pt -thermocouples was used. Tm_2O_3 (99.996%), H_3BO_3 (A.C.S. grade) and MgO (A.C.S. grade) were used as crystal-forming agents for the solid-state synthesis of polycrystalline TmMB. Calculated amounts of Tm_2O_3, MgO, H_3BO_3 were weighted, mixed together, and pressed into tablets 15 mm in diameter. The compact TmMB tablets were heated in an alundum crucible at the temperature of 900 °C during 72 hours, and then a furnace was gradually cooled to room temperature.

In solid-phase synthesis, crystal-forming components were initially weighed corresponding to the composition of $TmMgB_5O_{10}$. As a result, only the $TmBO_3$ phase was formed. According to the Le Chatelier principle, an excess of one of the components shifts the direction of the reaction towards the formation of the desired phase. Further experiments were carried out using non-stoichiometric load with 100% excess of MgO. This approach led to the formation of a nearly monophase $TmMgB_5O_{10}$ sample at 900 °C.

 doi:10.20944/preprints202308.2036.v1

Spontaneous TmMB crystals were obtained from high-temperature $K_2Mo_3O_{10}$-based flux melt. The $K_2Mo_3O_{10}$ solvent used was a stoichiometric mixture of K_2MoO_4 (A.C.S. grade) and MoO_3 (A.C.S. grade). Previously synthesized by solid-state technique TmMB was taken as crystal-forming component. Thoroughly mixed starting charge with a crystal phase-to-flux weight ratio of 30:70 wt.% was loaded into a 15 ml platinum crucible, placed in a furnace, heated to 900 °C and held for 24 h to ensure complete homogenization of the solution. Subsequently, the flux melt was cooled to 800 °C at a rate of 1 °C/h, followed by cooling at 10 °C/h to 300 °C.

$K_2Mo_3O_{10}$ –based solvents seem to be the most suitable for growth of different borates crystals. Nevertheless $LnMgB_5O_{10}$ solids dissolve incongruently in a $K_2Mo_3O_{10}$ melt, and reactions between $K_2Mo_3O_{10}$ and $LnMgB_5O_{10}$ result in new crystalline phases, mostly, crystal-forming oxides, as well as $LnBO_3$. The formation temperatures of these co-crystallizing phases depend on the borate type and its concentration in a flux melt. Small crystals of co-existing phases that appeared at high temperatures become the nucleation centers of spontaneous $LnMgB_5O_{10}$ crystals upon cooling. As a result of the incongruent dissolution of LnMg-borate, the melt is enriched in B_2O_3 and Ln_2O_3. Rare-earth metal oxides, in turn, cause the formation of $LnBO_3$ with calcite- or vaterite-type structure depending on the temperature [15]. The temperature range for LnMB synthesis is restricted by the properties of $K_2Mo_3O_{10}$ –based high-temperature solutions and by borate stability in such a melt. Usually the melting temperature of the charge does not exceed 1050 °C because of the significant increase in the borate decomposition rate. The lower temperature boundary (commonly ~ 800 °C) is determined by a significant increase in melt viscosity with a corresponding decrease in the crystal growth rate.

The morphological features and elemental analysis were studied by analytical scanning electron microscopy (SEM) technique using JSM-IT500 microscope, JEOL Ltd., Japan, equipped with energy dispersive X-ray (EDX) detector X-Max-50, Oxford Instruments Ltd., GB (Laboratory of Analytical Techniques of High Spatial Resolution, Dept. of Petrology, Moscow State University).

Single-crystal X-ray studies were carried out by an Xcalibur diffractometer equipped with a CCD-detector (MoKα radiation). The XRD data were integrated using the CrysAlisPro program software [16]. Powder X-ray diffraction (PXRD) studies were carried out on a Rigaku MiniFlex-600 powder diffractometer (Rigaku Corp., Japan). PXRD datasets were collected in continuous mode at room temperature (CuKα radiation) in the range of 2θ = 3–90°, scan speed of 4° per minute.

Differential scanning calorimetry (DSC) measurements were performed by means of STA 449 F5 Jupiter equipment (Netzsch, Germany) in the temperature range of 50 – 1200 °C with a heating rate of 20 °C/min in Ar gas flow. A PtRh20 crucible of 85 µl volume was used in the DSC experiments.

The band structure for TmMB was calculated within the framework of density functional theory using the pseudopotential plane wave basis of a Quantum Espresso software package [17]. The electronic exchange-correlations were treated by the Perdew-Burke-Ernzerhof (PBE) under a generalized gradient approximation (GGA) [18]. Ultrasoft pseudopotentials were used to describe the interaction between electrons and ions [19]. The kinetic energy cut-off values of the wavefunctions were limited to 58 Ry. The integration calculation of the system in Brillouin region uses the monkhorst-pack scheme, the k grid point is 3 × 3 × 3 and the cut-off energy of plane wave of the system is set at 750 eV to ensure the convergence of energy and configuration of the system at the level of quasi-complete plane wave base. In the self-consistent field operation, Pulay density mixing method is adopted, and the self-consistent field is set as 1×10^{-6} eV/atom. The calculations did not include spin–orbit coupling. Full relativistic effects were taken for the nucleus states, and the scalar relativistic approximation was used for the valence states.

A Cary Eclipse (Agilent Technologies) fluorescence spectrometer equipped with a 75 kW xenon light source (pulse length $\tau = 2\mu$s, pulse frequency ν = 80 Hz, wavelength resolution 0.5 nm; PMT Hamamatsu R928) was used to record photoluminescence emission (PL) and excitation (PLE) spectra. All measurements were performed at room temperature and corrected for the sensitivity of the spectrometer. The quantum yield defined as the ratio of the number of emitted photons to the number of photons absorbed (QY, %) for visible region was measured on an Edinburgh Instruments FS5

Preprints (www.preprints.org) | NOT PEER-REVIEWED | Posted: 30 August 2023 doi:10.20944/preprints202308.2036.v1

spectrofluorometer equipped with a SC-30 integrating sphere module and a Hamamatsu PMT R928P. The measurement was provided at room temperature.

Luminescence emission spectra under heating upon 500 K with the excitation in the UV region were measured using a 150 W xenon lamp (Oriel Instruments, Stratford, USA) as an excitation source, an MDR-206 primary monochromator (Lomo, Saint-Petersburg, Russia) and a LOT-Oriel MS-257 spectrograph (Oriel Instruments, Stratford, USA) equipped with a Marconi CCD detector (Marconi Applied Technologies Limited, Chelmsford, England). Samples were mounted into a Cryotrade LN-120 vacuum optical cryostat (Cryotrade engineering, Moscow, Russia).3. Results and Discussion

Spontaneous isometric crystals up to 1 mm in size were obtained from $K_2Mo_3O_{10}$-based flux melt (Figure 1). Preliminary XRD studies were performed to find the sample with the best diffraction reflection profile for single-crystal X-ray study. As follows from these pre-experiments, all tested specimens were crystal clusters or twin crystals.

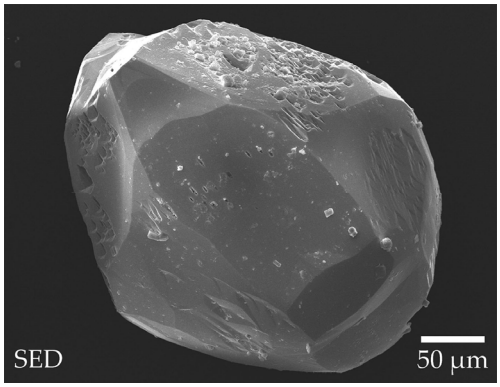

Figure 1. $TmMgB_5O_{10}$ spontaneous crystals grown from $K_2Mo_3O_{10}$-based system.

Qualitative energy-dispersive X-ray analysis showed peaks corresponding to thulium, magnesium, boron and oxygen (Figure 2).

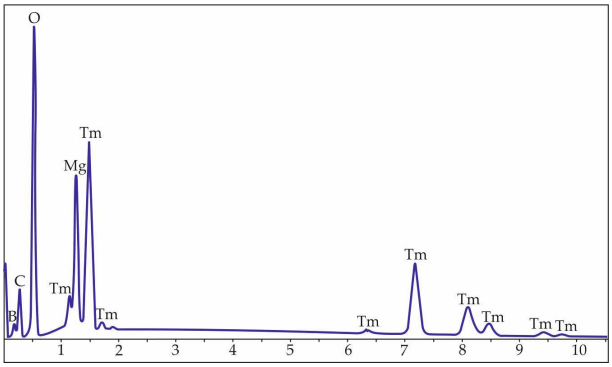

Figure 2. Energy-dispersive X-ray qualitative analysis of TmMg-borate crystal.

Diffraction patterns of $TmMgB_5O_{10}$ were analyzed by the CrysAlis software [16]. As a result, reflexes corresponding to two components with close unit cell parameters $a_1 = 8.476(1)$ Å, $b_1 = 7.577(1)$ Å, $c_1 = 9.368(1)$ Å, $a_2 = 8.474(2)$ Å, $b_2 = 7.572(2)$ Å, $c_2 = 9.361(2)$ Å were reveal. No rigid regularities of the mutual orientation of the bases of these components, associated with a significant change in the size of the unit cell or sp. gr. (superstructure), have been found (Figure 3).

Preprints (www.preprints.org) | NOT PEER-REVIEWED | Posted: 30 August 2023 doi:10.20944/preprints202308.2036.v1

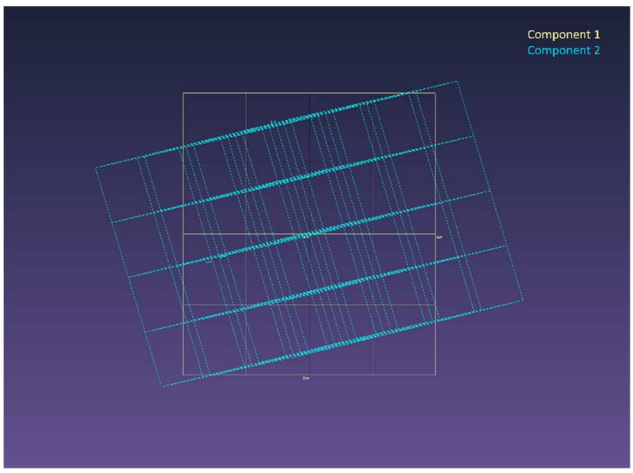

Figure 3. Mutual orientation of two monoclinic components of Tm in reciprocal space.

The relationship between the components can be represented by following vector equations:
$\boldsymbol{a}$ = (-0.711 × $\boldsymbol{a}$'-0.29 × $\boldsymbol{b}$'+0.547 × $\boldsymbol{c}$');
$\boldsymbol{b}$ = (0.578 ×$\boldsymbol{a}$'+0.136 × $\boldsymbol{b}$'+0.644 × $\boldsymbol{c}$');
$\boldsymbol{c}$ = (-0.258 ×$\boldsymbol{a}$'-1.199 × $\boldsymbol{b}$'-0.01 × $\boldsymbol{c}$').

The ratio of the two twin components is 75.1% and 23.0% of all registered reflections, respectively. The existence of two components for the TmMB single crystal slightly reduces the quality of the obtained structural model and leads to overestimated structure refinement factors. The model proposed is obtained from the experimental data of the first component (75.1% of the total number of reflections). It is not possible to correctly solve and refine the crystal structure of the second component due to the extremely high value of the parameter R_{int2} = 79%.

The crystal structure model was determined and refined using the Jana2020 software package [20]. Structural patterns similar to those described in the literature [21,22] were obtained using the SuperFlip utility [23] within the *sp.gr*. $P2_1/n$. The experimental and crystallographic data and structural refinements of TmMB are summarized in Table 1.

Table 1. Crystallographic data, details relating to X-ray data collection and structure refinements of $TmMgB_5O_{10}$.

Chemical formula	**$TmMgB_5O_{10}$**
Sp.gr., Z	$P2_1/n$, 4
a, *b*, *c*, Å	8.476(1) 7.577(1) 9.368(1)
β, °	94.035(3)
V, Å	600.1(1)
D, g/cm^3	4.508
Radiation; *λ*, Å	MoK_α; 0.71069
μ, mm^{-1}	14.946
T, K	295
Diffractometer	Xcalibur
Scan type	ω
Absorption coefficient; T_{min}/T_{max}	By cut; 0.125/1.000
θ_{max}, °	30.61
Limitation of *h*, *k*, *l*	$-11 \le h \le 12$; $-10 \le k \le 10$; $-12 \le l \le 13$

Preprints (www.preprints.org) | NOT PEER-REVIEWED | Posted: 30 August 2023 doi:10.20944/preprints202308.2036.v1

The number of reflections: measured/ independent ($N1$) / I > 3σ(I) ($N2$)	8445 / 1601 / 1303
R_{int}, %	19.2
The method of refinement	OLS by F2
The number of refined parameters	71
Consideration of extinction, k	Type 2
R_1/R_{w2} on $N1$	0.0543/0.1045
R_1/R_{w2} on $N2$	0.0638/0.1056
S	2.42
$\Delta\rho_{min}/\Delta\rho_{max}$	–5.54 / 5.50

The model of the structure consists of 17 independent atomic positions: one thulium position (Tm1), one magnesium position (Mg1), five boron atom positions (B1-B5) and ten oxygen positions (O1-O10). The low quality of the crystal and, as a result, of the diffraction experiment does not allow one to refine the parameters of anisotropic atomic displacements, which affects the value of the structure refinement factors and the values of the residual electron density. The atomic displacement parameters were refined isotropically for all localized positions; the occupancy of all positions is 100% (Table 2). The principle interatomic distances are listed in Table 3.

Table 2. Atomic coordinates and equivalent isotropic thermal parameters U_{eq} in the $TmMgB_5O_{10}$ structure.

Atom	***x/a***	***y/b***	z/c	U_{eq}, Å^2
Tm1	0.3152(1)	0.6865(1)	0.2582(1)	0.0065(1)
Mg1	0.596(1)	0.406(1)	0.130(1)	0.005(1)
B1	0.335(1)	0.898(1)	0.491(1)	0.006(1)
B2	0.436(1)	0.186(1)	-0.089(1)	0.006(1)
B3	-0.084(1)	0.573(1)	0.254(1)	0.008(1)
B4	0.517(1)	0.676(1)	0.602(1)	0.003(1)
B5	0.224(1)	-0.034(1)	-0.056(1)	0.006(1)
O1	0.250(1)	0.945(1)	0.370(1)	0.006(1)
O2	0.320(1)	0.124(1)	-0.011(1)	0.007(1)
O3	0.812(1)	0.532(1)	0.121(1)	0.006(1)
O4	0.682(1)	0.150(1)	0.140(1)	0.006(1)
O5	0.451(1)	0.770(1)	0.475(1)	0.007(1)
O6	0.508(1)	0.350(1)	-0.073(1)	0.006(1)
O7	0.490(1)	0.093(1)	-0.201(1)	0.008(1)
O8	0.583(1)	0.472(1)	0.351(1)	0.007(1)
O9	0.038(1)	0.705(1)	0.228(1)	0.002(1)
O10	0.677(1)	0.611(1)	0.580(1)	0.007(1)

Table 3. The main interatomic distances (Å) in the $TmMgB_5O_{10}$ structures.

Atoms	**Distance, Å**	**Atoms**	**Distance, Å**
Tm1 – O1	2.304(7)	B2 – O2	1.347(13)
Tm1 – O1	2.236(7)	B2 – O6	1.387(12)
Tm1 – O2	2.747(7)	B2 – O7	1.363(13)
Tm1 – O5	2.354(7)	**<B2 – O>**	1.365
Tm1 – O6	2.389(7)	B3 – O3	1.512(12)
Tm1 – O7	2.441(7)	B3 – O4	1.456(13)
Tm1 – O8	2.875(6)	B3 – O7	1.452(13)
Tm1 – O9	2.355(6)	B3 – O9	1.467(12)
Tm1 – O10	2.713(7)	**<B3 – O>**	1.472

Preprints (www.preprints.org) | NOT PEER-REVIEWED | Posted: 30 August 2023 doi:10.20944/preprints202308.2036.v1

Tm1 – O10	2.497(1)	B4 – O5	1.462(12)
<Tm1 – O>	2.4911	B4 – O8	1.492(12)
Mg1 – O3	2.067(7)	B4 – O9	1.485(12)
Mg1 – O4	2.071(8)	B4 – O10	1.472(12)
Mg1 – O6	2.040(7)	**<B4 – O>**	1.478
Mg1 – O6	2.104(7)	B5 – O2	1.490(12)
Mg1 – O8	2.137(7)	B5 – O4	1.455(13
Mg1 – O9	2.371(7)	B5 – O8	1.504(11)
<Mg1 – O>	2.131	B5 – O10	1.483(13)
B1 – O1	1.347(12)	**<B5 – O>**	1.483
B1 – O3	1.353(13)		
B1 – O5	1.398(12)		
<B1 – O>	1.366		

The thulium cations are coordinated by ten O atoms, forming distorted polyhedra that share a common edge and form one-dimensional zigzag chains extending along *b* axis (Figure 4*a*). Magnesium atoms are located inside oxygen octahedra that form shared-by- edge dimeric Mg_2O_{10} groups. The adjacent Tm-O chains are linked together by dimeric Mg_2O_{10}, building Tm-Mg-O layers (Figure 4*b*). Boron atoms have a mixed coordination (3t+2Δ): three B atoms are located inside oxygen tetrahedra and the other two B atoms are coordinated by three O atoms, forming planar triangle. BO_4-tetrahedra and BO_3-triangles connected by corners form pentaborate cluster [1]. Each B_5O_{12} unit *via* corner-sharing O atom between two neighboring clusters form 4-memred rings, from which infinite two-dimensional B-O layers are further assembled (Figure 4*c*). Countless boron-oxygen layers are linked together by Tm and Mg cations forming rigid three-dimensional framework (Figure 4*d*).

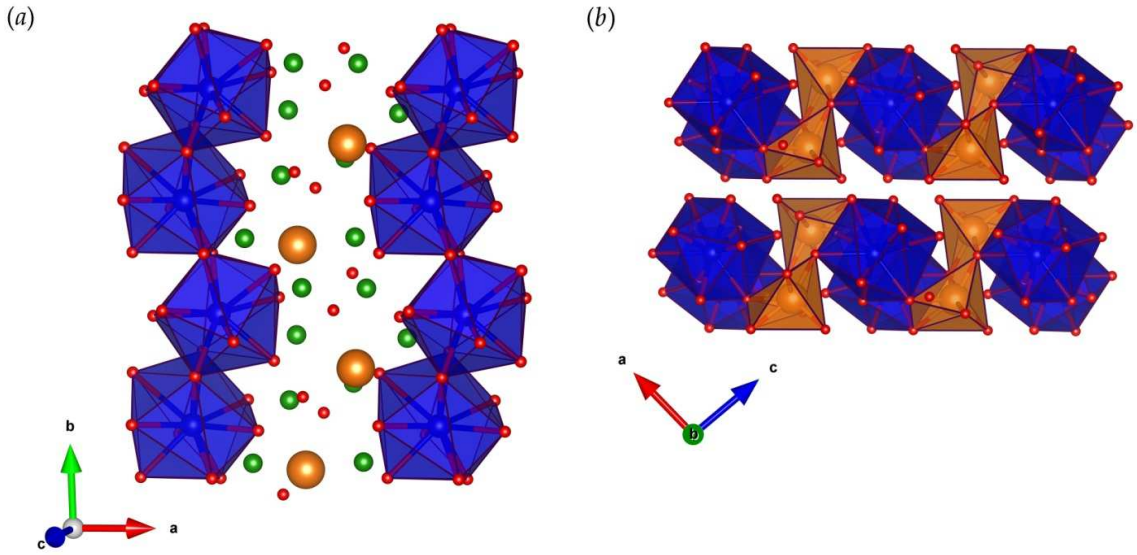

Preprints (www.preprints.org) | NOT PEER-REVIEWED | Posted: 30 August 2023 doi:10.20944/preprints202308.2036.v1

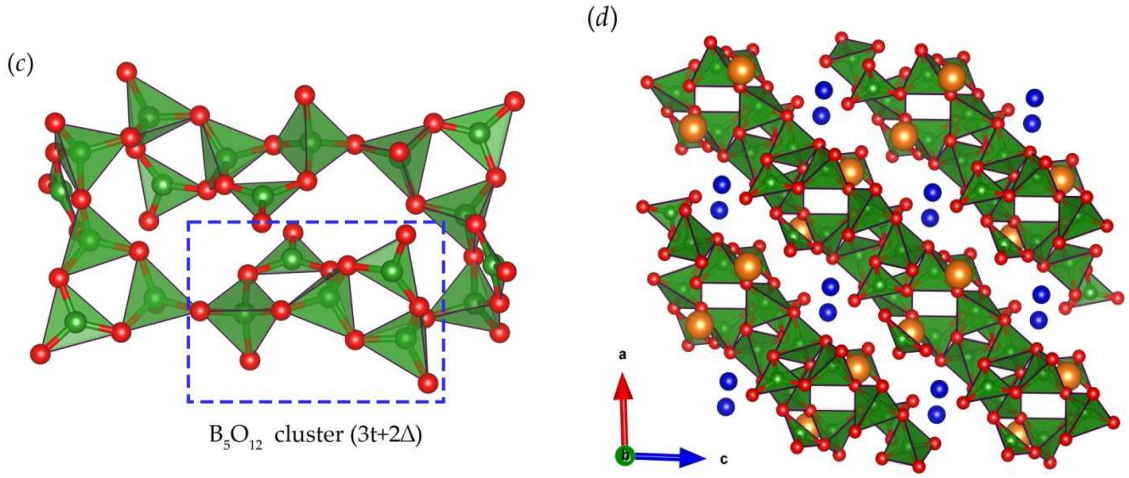

Figure 4. Structure of $TmMgB_5O_{10}$: (**a**) zigzag chains of edge-share TmO_{10} distorted polyhedral extending along *b* axis; (**b**) Tm-Mg-O layers, formed by linked Tm-O chains and dimeric Mg_2O_{10} clusters, projection along *b* axis, (**c**) 4-membered ring assembled from B_5O_{12} neighboring clusters, (**d**) two-dimensional B-O layers, linked together by Tm and Mg cations, projection along *b* axis. The blue, orange, green and red balls represent Tm, Mg, B and O respectively. Visualization by VESTA [24].

To determine the behavior and melting temperature of TmMg-borate, DSC measurements were performed. The calorimetric data in the temperature range of 50-1200 °C are shown in Figure 5. The DSC heating curve for the sample feature one sharp endothermic peak with the onset temperature of ~1020 °C, but no exothermal peak was observed on the cooling curve. After melting, the residue was characterized by PXRD analysis, which showed that it was different from the initial compound powder, and the decomposition products of TmMB compound are a mixture of $TmBO_3$ and $Mg_2B_2O_5$. These results agreed with previously obtained for Yb:$YMgB_5O_{10}$ crystals [25].

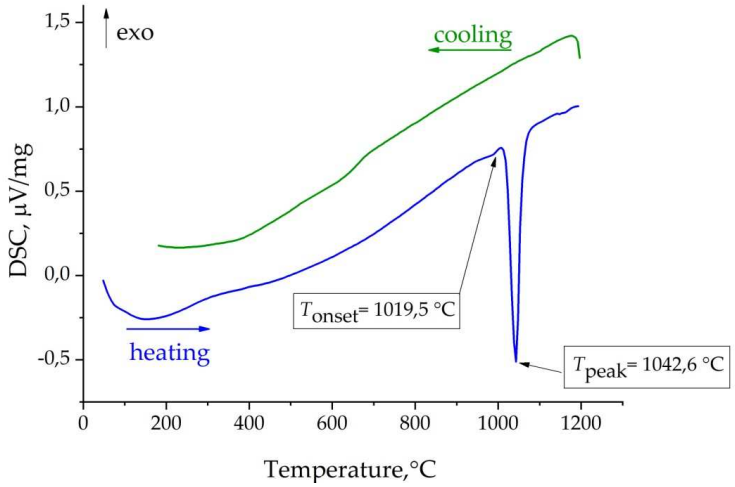

Figure 5. DSC curve of $TmMgB_5O_{10}$ compound in the temperature range of 50-1200 °C.

The PXRD dataset was collected to confirm that the crystal structure is representative for the entire experimental sample. The pattern fits well with that calculated from the cif-file obtained from the structural studies and calculated from cif-file of $YMaB_5O_{10}$ (ICSD #4489) (Figure 6).

Preprints (www.preprints.org) | NOT PEER-REVIEWED | Posted: 30 August 2023 doi:10.20944/preprints202308.2036.v1

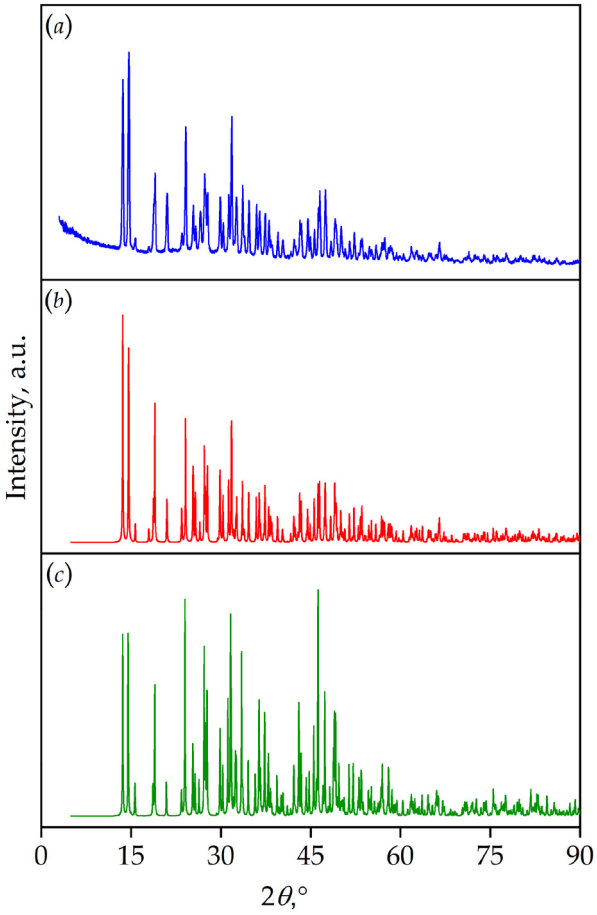

Figure 6. PXRD patterns (*a*) of $TmMgB_5O_{10}$ solids, (*b*) calculated from the cif-file obtained from structural studies of single crystal, and (*c*) calculated from the cif-file of $YMgB_5O_{10}$ (ICSD #4489).

The band structure of the TmMB material was calculated to find out the electronic characteristics of the $TmMgB_5O_{10}$ model structure (Figure 7). The outcome of this analysis shows that TmMB is an insulator, as evidenced by the determination of an indirect energy gap of about 6.37 eV. This gap was determined by the A point at the maximum of the valence bands (VBM) and the Γ point at the minimum of the conduction band (CBM). However, it should be noted that GGA calculations have been shown to underestimate band gaps, and therefore, the experimental band gap for $MgTmB_5O_{10}$ may differ slightly from the calculated value. Notably, the VBM is a flat band, and the maximum values at Γ and A points in the Brillouin zone are quite close. This suggests that even a small concentration of defects in the simulated crystal structure could result in a direct band gap at the Γ point.

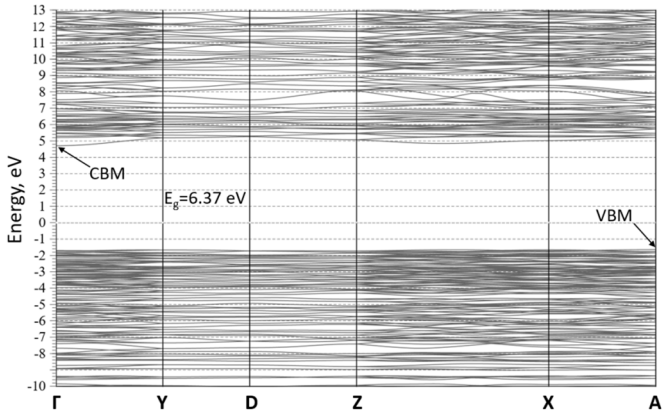

Figure 7. The calculated band structure of $MgTmB_5O_{10}$.

Preprints (www.preprints.org) | NOT PEER-REVIEWED | Posted: 30 August 2023 doi:10.20944/preprints202308.2036.v1

According to the calculated density of states (DOS) of $MgTmB_5O_{10}$ (Figure 8), the electronic structure in energy range from −28.0 to 22 eV mainly comprises Tm-*s* and O-*s*/*p* states with smaller contributions from B-*s*/*p* and Mg-*s*/*d*/*p* states. The significant contribution to the lower conduction band comes from the Tm-*d* state, while O-*s* in the upper VB has considerable effect on the dispersion.

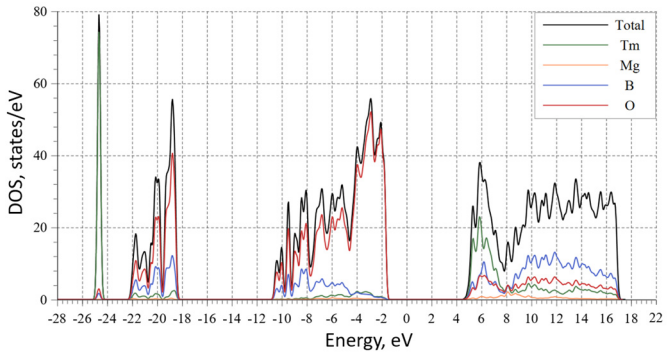

Figure 8. The calculated density of states of $MgTmB_5O_{10}$.

The normalized to photoluminescence excitation and photoluminescence emission spectra of the $TmMgB_5O_{10}$ compound are shown in Figure 9. On the PLE spectrum (Figure 9*a*) for $TmMgB_5O_{10}$ the typical transition of Tm^{3+} ion is observed in near ultra-violet region. The sharp line with maxima centered at 358 nm corresponds to transition $^3H_6 \rightarrow {}^1D_2$ [26]. Since the indirect energy gap is about 6.37 eV, excitation with such higher transition energies is not possible in the 220 - 340 nm range. The standard sharp lines for Tm^{3+} were registered for PL spectrum (Figure 9*b*). The maxima centered at 455, 479, 667 and 753 nm correspond to $_1D_2 \rightarrow {}^3F_4$, $^1G_4 \rightarrow {}^3H_6$, $^1G_4 \rightarrow {}^3F_4$ and $^3H_4 \rightarrow {}^3H_6$ transitions according to [27]. The most intensive transition is observed for $^1D_2 \rightarrow {}^3F_4$, which emitting in blue region. So, $MgTmB_5O_{10}$ demonstrates photoluminescence in blue spectral region. Additionally, the integral intensity is significantly low and takes a few arb. units. Such behavior can be explained to presence high concentration quenching effect in observed $TmMgB_5O_{10}$, which was registered in other hosts (see, for example, Refs. [28,29]. This is confirmed by minor value of QY approximately 3%. Such extremely low QY can indicate to concentration quenching through all the resonance channels of cross-relaxation "upward" and "downward" [30] in studied host. The calculating distance Tm-Tm in structure (approximate value is 3.94 Å) leads to registered concentration quenching. In spite of DFT calculations of the $MgTmB_5O_{10}$ band structure for an ideal crystal model showed that this material is an insulator, however, contrasting these results, experimental observations revealed a presence of PL peaks in the blue spectral range. Hence, it can be inferred that the presence of point defects in the crystal structure gives rise to additional electronic states. A similar conclusion was observed in [21], where the properties of $MgYB_5O_{10}$ compound where investigated. Furthermore, observed crystals exhibit thermal stability of photoluminescence (Figure 10). As the temperature increases, the total integral intensity of $^1D_2 \rightarrow {}^3F_4$ transition decreases slowly, indicating the standard thermal quenching of photoluminescence for $MgTmB_5O_{10}$. The thermal stability of photoluminescence in this Tm^{3+}-activated host is higher than in other hosts, for example, in crystals BaY_2F_8 [31] and powder $YNbO_4$ [32]. It should be noted that other transitions were not detected in temperature dependence because of their low intensity.

Preprints (www.preprints.org) | NOT PEER-REVIEWED | Posted: 30 August 2023 doi:10.20944/preprints202308.2036.v1

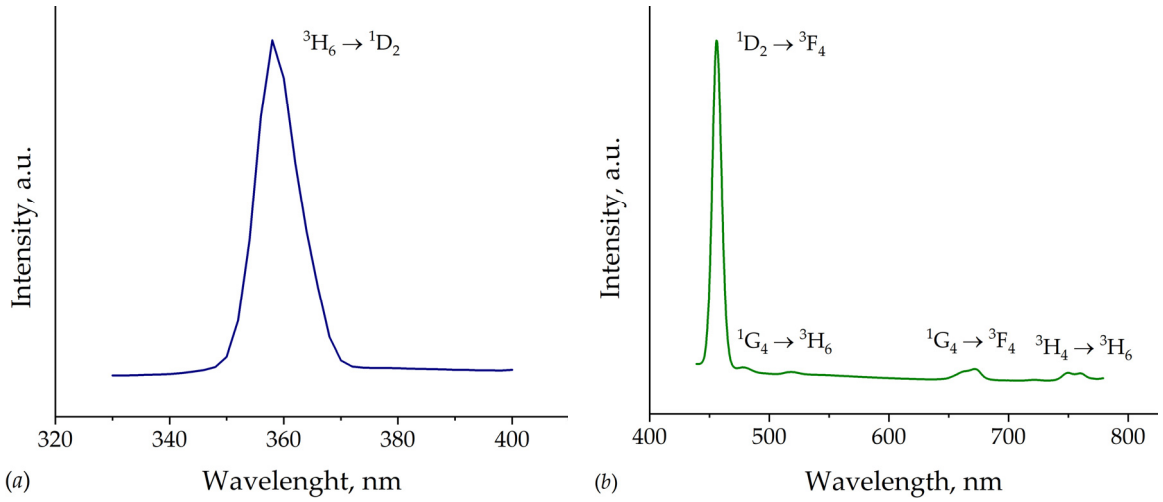

Figure 9. (**a**) PLE (λ_{em} = 455 nm) and (**b**) PL (λ_{em} = 358 nm) spectra for $MgTmB_5O_{10}$.

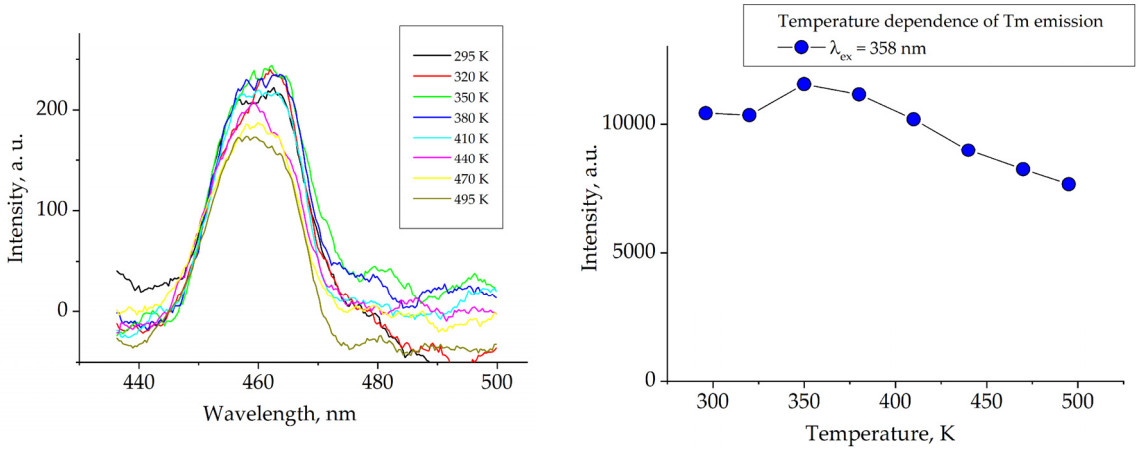

Figure 10. The temperature dependence of Tm^{3+} photoluminescence (λ_{em} = 358 nm); the right figure shows the relative emission intensity as a function of temperature.

4. Conclusions

Spontaneous crystals of $TmMgB_5O_{10}$ were synthesized by a two-step technique, where polycrystalline TmMB solids, previously obtained by solid-phase synthesis, were used as crystal-forming agent for flux growth from $K_2Mo_3O_{10}$-based system. Obtained solids crystallize in the sp. gr. $P2_1/n$ with unit cells parameters a= 8.476(1) Å, b=7.577(1) Å, c=9.368(1) Å, β=94.035(3)°, V=600.1(1) Å^3, and z=4. The electronic structure of $TmMgB_5O_{10}$ was calculated. A comprehensive study of TmMg-borate crystals was performed using scanning electron microscopy, DSC technique, and luminescence spectroscopy.

Author Contributions: conceptualization, E.A.V.; validation, E.A.V., V.V.M., A.M.A., D.V.D., I.V.N., E.I.M., D.D.M., V.L.K., V.O.Y., D.A.N. and E.V.K.; investigation, E.A.V., V.V.M., A.M.A., D.V.D., I.V.N., E.I.M., D.D.M., V.L.K., V.O.Y., D.A.N. and E.V.K.; resources, E.A.V., V.V.M., D.V.D., V.L.K. and V.O.Y.; writing—original draft preparation, E.A.V., A.M.A., D.V.D., I.V.N. and E.I.M.; writing—review and editing, E.A.V., A.M.A.; visualization, E.A.V.; supervision, E.A.V. All authors have read and agreed to the published version of the manuscript.

Funding: This research received no external funding.

Data Availability Statement: Cambridge Crystallographic Data Centre. CCDC reference 2286790.

Acknowledgments: X-ray diffraction data was performed using the equipment of the Shared Research Centre FSRC «Crystallography and Photonics» RAS within the State assignment FSRC «Crystallography and Photonics» RAS.

References

1. Leonyuk, N.I.; Maltsev, V.V.; Volkova, E.A. Crystal chemistry of high-temperature borates. *Molecules* **2020**, 25(10), 2450. https://doi.org/10.3390/molecules25102450.
2. Hölsä, J.; Leskelä, M. Fluorescence spectrum, energy level scheme and crystal field analysis of europium(+III) doped lanthanum magnesium borate $LaMgB_5O_{10}:Eu^{3+}$. *Molecular Physics* **1985**, *54(3)*, 657–667. https://doi.org/10.1080/00268978500100511.
3. Mitina, D.D.; Maltsev V.V.; Deineko, D.V.; Volkova E.A.; Koporulina E.V.; Kuzmin, N.N.; Kosorukov V.L.; Jiliaeva A.I. Luminescent properties of lanthanum-magnesium pentaborate crystals doped by Tb^{3+} and Eu^{3+} ions. *J. Inorganic chemistry* **2023**, *9* (in press).
4. Saubat, B.; Vlasse, M.; Fouassier, C. Synthesis and structural study of the new rare earth magnesium borates $LnMgB_5O_{10}$ (Ln = La, …, Er). *J. Solid State Chem*. **1980**, *34(3)*. 271–277. https://doi.org/10.1016/0022-4596(80)90425-9.
5. Fouassier, C.; Saubat, B.; Hagenmuller, P. Self-quenching of Eu^{3+} and Tb^{3+} luminescencein $LaMgB_5O_{10}$: a host structure allowing essentially one-dimensional interactions. *J. Lumin*. **1981**, *23*, 405-412. https://doi.org/10.1016/0022-2313(81)90143-5.
6. Saubat, B.; Fouassier, C.; Hagenmuller, P. Luminescent efficiency of Eu^{3+} and Tb^{3+} in $LaMgB_5O_{10}$ - type borates under excitation from 100 to 400 nm. *Mater. Res. Bull*. **1981**, *16*, 193-198. https://doi.org/10.1016/0025-5408(81)90081-7.
7. Knitel, M.J.; Dorenbos, P.; van Eijk, C.W.E.; Plasteig, B.; Viana, B.; Kahn-Harari, A.; Vivien, D. Photoluminescence, and scintillation/thermoluminescence yields of several Ce^{3+} and Eu^{2+} activated borates. *Nuclear Instruments and Methods in Physics Research A* **2000**, *443(2-3)*, 364–374. https://doi.org/10.1016/s0168-9002(99)01154-7.
8. Lin, C.K.; Yu, M.; Pang, M.L.; Lin, J. Photoluminescent properties of sol–gel derived $(La,Gd)MgB_5O_{10}:Ce^{3+}/Tb^{3+}$ nanocrystalline thin films. *Opt. Mater*. **2006**, *28(8-9)*, 913–918. https://doi.org/10.1016/j.optmat.2005.04.009.
9. El Jouhari, N.; Parent, C.; Le Flem, G. Photoluminescence of Ce^{3+}, Tb^{3+}, and Mn^{2+} in Glasses of Base Composition $LaMgB_5O_{10}$. J. *Solid State Chem*. **1996**, *123(2)*, 398–407. https://doi.org/10.1006/jssc.1996.0195.
10. Huang, Y.; Chen, H.; Sun, S.; Yuan, F.; Zhang, L.; Lin, Z.; Zhang, G.; Wang, G. Growth, thermal, spectral and laser properties of Nd:$LaMgB_5O_{10}$ crystal – A new promising laser material. *J. Alloys Compd*. **2015**, *646*, 1083–1088. https://doi.org/10.1016/j.jallcom.2015.06.196.
11. Sun, S.; Wei, Q.; Li, B.; Shi, X.; Yuan, F.; Lou, F.; Zhang, L.; Lin, Z.; Zhong, D.; Huang, Y.; Teng, B. The $YMgB_5O_{10}$ crystal preparation and attractive multi-wavelength emission characteristics of doping Nd^{3+} ions. *J. Mater. Chem. C*, **2021**, *9*, 1945; https://doi.org/10.1039/d0tc05372.
12. Huang, Y.; Lou, F.; Sun, S.; Yuan, F.; Zhang, L.; Lin, Z.; You, Z. Spectroscopy and laser performance of Yb^{3+}:$GdMgB_5O_{10}$ crystal. *J. Lumin*. **2017**, *188*, 7–11. https://doi.org/10.1016/j.jlumin.2017.03.070.
13. Mitina, D.D.; Maltsev, V.V.; Leonyuk, N.I.; Gorbachenya, K.N.; Deineka, R.V.; Kisel, V.E.; Yasukevich, A.S.; Kuleshov, N.V. Growth and Characterization of $RMgB_5O_{10}$ (R = Y, La, Gd) Crystals. *Inorg. Mater.* **2020**, *56(2)*, 211–222. https://doi.org/s0020168520020132 .
14. Maltsev, V.V.; Mitina, D.D.; Belokoneva E.L., Volkova, E.A.; Koporulina E.V.; Jiliaeva, A.I. Synthesis and flux-growth of rare-earth magnesium pentaborate crystals $RMgB_5O_{10}$ (*R*=Y, Gd, La, Tm and Yb). *J. Cryst. Growth* **2022**, *587*, 126628. https://doi.org/10.1016/j.jcrysgro.2022.126628.
15. Leonyuk, N.I.; Leonyuk, L.I. Growth and characterization of $RM_3(BO_3)_4$ crystals. *Progr. Cryst. Growth Charact.* **1995**, *31*, 179-278. https://doi.org/10.1016/0960-8974(96)83730-2.
16. Rigaku Oxford Diffraction, CrysAlis Pro Software System, Version 1.171.64.119a, Rigaku Corporation, Oxford, UK, 2018.
17. Giannozzi, P.; Baroni, S.; Bonini, N. *et al*. QUANTUM ESPRESSO: a modular and open-source software project for quantum simulations of materials. *J. Phys. Condens. Matter* **2009**, *21*(39), 395502. https://doi.org/10.1088/0953-8984/21/39/395502.
18. Perdew, J.P.; Burke,K.; Ernzerhof, M. Generalized Gradient Approximation Made Simple. *Phys. Rev. Lett.* **1996**, *77(18)*, 3865–3868. https://doi.org/10.1103/physrevlett.77.3865.
19. Lin, J.S.; Qteish, A.; Payne, M. C.; Heine, V. Optimized and transferable nonlocal separableab initiopseudopotentials. *Phys. Review B* **1993**, *47(8)*, 4174–4180. https://doi.org/10.1103/physrevb.47.4174.
20. Petricek, V.; Dusek, M.; Palatinus L. Crystallographic Computing System JANA2006: General features, *Z. Kristallogr*. **2014**, *229*, 345-352. https://doi.org/10.1515/zkri-2014-1737.

21. Zhang, J.; Tao, X.; Cai, G.; Jin, Z. Phase relation, structure, and properties of borate $MgYB_5O_{10}$ in MgO–Y_2O_3–B_2O_3 system. *Powder Diffraction* **2017**, *32(02)*, 97–106. https://doi.org/10.1017/s0885715617000227.
22. Huang, Y.; Zhou, W.; Sun, S.; Yuan, F.; Zhang, L.; Zhao, W.; Wang, G.; Lin, Z. Growth, structure, spectral and laser properties of Yb3+:LaMgB5O10– a new laser material. *CrystEngComm* **2015**, *17(38)*, 7392–7397. https://doi.org/10.1039/c5ce01443c.
23. Palatinus, L. Ab initio determination of incommensurately modulated structures by charge-flipping in super space. *Acta Cryst. A* **2004**, *60*, 604–610. https://doi.org/10.1107/S0108767304022433.
24. Momma, K.; Izumi, F. VESTA 3 for three-dimensional visualization of crystal, volumetric and morphology data. *J. Appl. Crystallogr.* **2011**, *44*, 1272-1276. https://doi.org/10.1107/S0021889811038970.
25. Gorbachenya, K.N.; Yasukevich, A.S.; Lazarchuk, A.I.; Kisel, V.E.; Kuleshov, N.V.; Volkova, E.A.; Maltsev, V.V.; Koporulina, E.V.; Yapaskurt, V.O.; Kuzmin, N.N.; et al. Growth and Spectroscopy of Yb:YMgB5O10 Crystal. *Crystals* **2022**, *12*, 986. https://doi.org/10.3390/cryst12070986
26. Yao, L.; Chen, G.; Yang, T.; Yuan, C.; Zhou, C. Energy transfer, optical and luminescent properties in Tm^{3+}/Tb^{3+}/Sm^{3+} tri-doped borate glasses. *J. Mater. Sci. Mater. Electron.* **2016**, *28(1)*, 553–558. https://doi.org/10.1007/s10854-016-5558-2.
27. Kuwik, M.; Kowalska, K.; Pisarska, J.; Pisarski, W.A. Spectroscopic Properties of Pr^{3+}, Tm^{3+}, and Ho^{3+} in Germanate-Based Glass Systems Modified by TiO_2. *Materials* **2023**, *16*, 61. https://doi.org/10.3390/ma16010061.
28. Borrego-Pérez, J.A.; González, F.; Meza-Avendaño, C.A.; De Los Santos, I.M.; López-Juárez, R.; Hernández, I.; Alonso-Guzman, E.M.; Martinez-Molina, W.; Chavez-Garcia, H.L. Structural, optical and photoluminescence properties of TiO_2 and TiO_2: Tm^{3+} nanopowders. *Optik* **2020**, 166083. https://doi.org/10.1016/j.ijleo.2020.166083.
29. Guerbous, L.; Derbal, M.; Chaminade, J.P. Photoluminescence and energy transfer of Tm^{3+} doped $LiIn(WO_4)_2$ blue phosphors. J. *Lumin.* 2010, *130(12)*, 2469–2475. https://doi.org/10.1016/j.jlumin.2010.08.014.
30. Kozhan, T.M.; Kuznetsova, V.V.; Pershukevich, P.P.; Sergeev, I.I.; Khomenko, V.S.; Chernyavskii, V.A. Concentration dependence of the quantum yield of luminescence of Tm^{3+} ions in gadolinium oxychloride. *J. Appl. Spectrosc.* **2004**, *71(6)*, 829–836. https://doi.org/10.1007/s10812-005-0009-5.
31. Makhov, V.N.; Uvarova, T.V.; Kirm, M.; Vielhauer, S. Thermal quenching of luminescence of BaY_2F_8 crystals activated with Er^{3+} and Tm^{3+} ions. *Bulletin of the Lebedev Physics Institute* **2016**, *43(12)*, 348–351. https://doi.org/10.3103/s1068335616120022.
32. Wang, X.; Li, X.; Xu, S.; Yu, H.; Zhang, J.; Zhang, X.; Cao, Y.; Cheng, L.; Sun, J.; Chen, B. Temperature-dependent luminescence properties of Dy^{3+}, Tm^{3+} single-/co-doped $YNbO_4$ phosphors. *Optik* **2021**, *238*, 166524. https://doi.org/10.1016/j.ijleo.2021.166524.